Journal of Molecular Structure 1293 (2023) 136291

Contents lists available at ScienceDirect

Journal of Molecular Structure

journal homepage: www.elsevier.com/locate/molstr

3D Ag(I) coordination polymer sandwiched by water-muconate anionic layers: Synthesis, structure, Hirshfeld surface analysis, binding with BSA, and photocatalytic activity

Laxmikanta Nandi [a], Shovan Barman [a], Arindam Das [a], Paula Brandão [b], Ennio Zangrando [c], Anirban Basu [a,*], Sudipta Dalai [a,*]

[a] Department of Chemistry, Vidyasagar University, Midnapore, West Bengal 721102, India
[b] Departamento de Química, CICECO-Instituto de Materiais de Aveiro, Universidade de Aveiro, Aveiro 3810-193, Portugal
[c] Department of Chemical and Pharmaceutical Sciences, University of Trieste, Trieste 34127, Italy

ARTICLE INFO

Keywords:
3D Silver(I) coordination polymer
Harshfeld surface analysis
BSA binding
Photocatalytic property

ABSTRACT

The sonochemical reaction between silver salt, 1,3-bis(4-pyridylpropane (bpp) and *trans,trans*-muconic acid (H_2muc) formed an Ag(I) coordination polymer with a 3D supramolecular sandwich architecture, {[Ag_8(bpp)$_8$(H_2O)$_3$].(muc)$_4$.29(H_2O)}$_n$, (**1**) consisting of the silver-bpp cationic host that alternates with 2D water–muc guest anionic layers. The latter is formed by H-bonded water molecules-anions comprising hexagonal (H_2O)$_6$ clusters. The Hirshfeld surface and fingerprint plots have been used to quantify the weak intermolecular interactions in the crystal packing arrangement. The study showed that intermolecular hydrogen bonds are the most critical in constructing the titled supramolecular complex, accounting for 51.2% of the total Hirshfeld surface. Several spectrofluorimetric methods have been employed to investigate the binding interaction between Bovine Serum Albumin (BSA) and the titled complex. The complex induced significant fluorescence quenching of BSA, indicating a strong binding affinity for the protein. Static or ground state complex formation was envisaged as the primary quenching mechanism when the complex interacts with BSA. In addition, the Ag compound also offers photocatalytic properties by degrading the toxic organic methylene blue dye.

1. Introduction

The importance of coordination polymers (CPs) in materials science is rapidly increasing [1]. Coordination polymers have drawn attention due to their attractive architectures [2] and potential applications in luminescence, magnetic materials, gas storage, non-linear optics, LEDs, conducting materials, heterogeneous catalysis, and antibacterial materials [3–12]. The d^{10} electronic configuration of silver(I) in coordination polymers offers several coordination numbers and diverse coordination geometries around the metal center [13,14]. Silver ions can give rise to coordination polymers with suitable polydentate neutral/ionic N and O-containing organic ligands [13,14], and 1,3-bis(4-pyridylpropane) is an effective neutral ligand for building these assemblies that continue to fascinate for the structural diversity and potential physical and chemical functions [15,16]. The formation of supramolecular structures in these coordination polymers is favored by non-covalent interactions, like argentophilic (Ag….Ag) interactions [17], hydrogen bonding, π-stacking, and self-assembly of metal ions [18]. Generally, heterocyclic systems are the building blocks for various physiologically significant and naturally occurring chemicals. As a result, Metal coordinated heterocyclic polymers are frequently used as building blocks for catalysis, medicinal chemistry, material science, and nanotechnology. And these compounds have been shown to have biological properties like interacting with BSA [18]. Bovine serum albumin (BSA) is the most investigated protein having a wide range of physiochemical, biochemical, and biophysical functions [19,20]. It plays an active role in the binding, transporting, and delivering steroids, fatty acids, porphyrins, food colors, and different types of drugs [21–23]. This multifunctional serum albumin is homologous to human serum albumin (HSA) with structurally similar three domains (I, II & III) [24]. Since BSA and HSA have excellent ligand adaptability, the binding and transportation of any drug are investigated by utilizing these proteins as model systems in interdisciplinary research fields such as pharmaceutical chemistry, biophysics, clinical physiology, *etc* [25].

* Corresponding authors.
E-mail addresses: anirbanbasu@mail.vidyasagar.ac.in (A. Basu), sudipta@mail.vidyasagar.ac.in (S. Dalai).

https://doi.org/10.1016/j.molstruc.2023.136291
Received 29 May 2023; Received in revised form 20 July 2023; Accepted 24 July 2023
Available online 25 July 2023

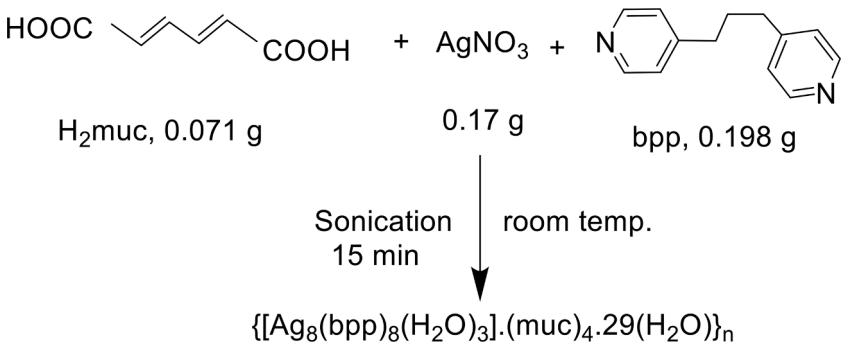

Scheme 1. Synthesis of Complex **1**.

On the other hand, industrial water treatment has become one of the significant environmental issues in recent years. In this connection, catalytic photodegradation is a potential approach for treating and purifying wastewater because it can mineralize organic contaminants into organic chemicals [26–31]. Different low-cost procedures, including filtering, biological treatment, activated charcoal adsorption, coagulation, and reverse osmosis, have proven ineffective, as the created solid wastes cause further pollution and environmental hazards . Catalytic photodegradation, sometimes known as "green technology," is one of the promising strategies for breaking harmful organic pollutants because of its trouble-free operation conditions and low prices [32]. Some silver (I) coordination polymers have been effectively applied as a catalyst in the decomposition of dyes [33–35].

Considering the considerations mentioned earlier, in the present work, we report the synthesis of a new Ag(I) coordination polymer and its binding ability to interact with the BSA protein using multiple spectrofluorimetric methods. In addition, we thoroughly studied the coordination polymer's catalytic property in connection with methylene blue's degradation. This toxic and carcinogenic organic dye can cause a severe threat to human health and environmental safety.

2. Experimental

2.1. Chemicals

Silver nitrate ($AgNO_3$), *trans, trans*-muconic acid (muc), 1,3-bis(4-pyridylpropane) (bpp) methylene blue, ($C_{16}H_{18}ClN_3S.xH_2O$), and methanol (CH_3OH) were of high purity and purchased from Sigma Aldrich India. All other chemicals were commercially purchased and used without further purification.

2.2. Instrumentation

Elemental analyses (C, H, and N) were performed using a PerkinElmer 240C analyzer. Absorption spectral studies were recorded on a Shimadzu Pharma specUV-1800 spectrophotometer (Shimadzu Corporation, Kyoto, Japan) at 25 °C using a paired 1 cm light path length quartz cuvettes, a 3 cm^3 volume were used for all measurements.

FT-IR spectra were collected using a Perkin-Elmer Spectrum, two FT-IR spectrophotometers equipped with a diamond head attenuated total reflectance (ATR) accessory, $LiTaO_3$ detector, and a KBr beam splitter at room temperature (Perkin Elmer, Inc., USA). All fluorescence spectral studies were recorded on Hitachi F-7000 Spectro-fluorimeter in a 1 cm (path length) quartz cell at 25 °C. Fluorescence lifetime data were collected using the Delta Flex™ Modular Fluorescence Lifetime system (Horiba Scientific, UK). Decay data were counted by time-correlated single photon counting (TCSPC) procedure. The actual data were evaluated with EZ-time software. Thermogravimetric analysis (TGA) was carried out using a Perkin Elmer Pyris Diamond TG/DTA thermal analyzer. The powder X-ray diffraction (PXRD) was performed on a Bruker D8 Advance X-ray diffractometer at a scan rate of 2° per minute.

2.3. Synthesis of $\{[Ag_8(bpp)_8(H_2O)_3].(muc)_4.29(H_2O)\}_n$ (1)

A mixture of *trans, trans*-muconic acid (0.071 g, 0.5 mmol), silver nitrate (0.17 g, 1 mmol), and 1,3-bis(4-pyridyl propane) (0.198 g, 1 mmol) was dissolved in 1:1 methanol-water mixture (20 mL) into a 50 mL round bottom flask. The mixture was treated for 15 min at ambient temperature under ultrasonic irradiation (160 W, 40 kHz). An aqueous NH_3 solution (25%) was added dropwise to the turbid solution resulting in a clear solution that was kept in the dark for five days to get diffraction-quality colorless single crystals of complex **1** (Scheme 1). Yield: 81%. Anal. Calc. For $C_{128}H_{192}Ag_8N_{16}O_{48}$ (M = 3585.92): C,42.86%, H, 5.39%, N, 7.42%, Found: C, 42.90%, H, 5.38%, N, 7.45%.

2.4. Crystallographic data collection and refinement

Data collection of complex **1** was carried out at 150(2) K on a Bruker APEX-II CCD diffractometer, all equipped with Mo-Kα graphite monochromatized radiation (λ = 0.71073 Å). Cell refinement, indexing, and scaling of the data set were carried out using Bruker APEX2 and Bruker SAINT packages [36]. The structure was solved using the direct method and subsequent Fourier analyses [37] and refined by the full-matrix least-squares method based on F^2 with all observed reflections [38]. Hydrogen atoms were placed at calculated positions except for water molecules on the difference Fourier map with some O-H distances restrained at 0.85(1) Å. Calculations were performed using the WINGX package [38] and molecular graphics using the Diamond program [39].

Crystal data and details of refinement. **1**: $C_{128}H_{192}Ag_8N_{16}O_{48}$, M = 3585.92, monoclinic, space group $P\ 2_1/c$, a = 24.685(2), b = 17.9698 (15), c = 35.490(4) Å, β = 110.268(3)°, V = 14768(2) $Å^3$, Z = 4, Dc = 1.613 g/cm^3, μ(Mo-Kα) = 1.125 mm^{-1}, F(000) = 7328, θ max = 25.82°. Final *R*1 = 0.0832, *wR*2 = 0.1903, S = 1.097 for 1987 parameters and 28,304 unique reflections [*R*(int) = 0.0658], of which 22,803 with $I > 2\sigma(I)$, max positive and negative peaks in difference *F* map 3.820, –3.841 e. Å-3.

2.5. Harshfeld surface analysis

This analysis represents an attempt beyond the internuclear distances and angles, crystal packing diagrams with molecules represented *via* various models, and the identification of close contacts thought necessary, thereby fundamentally altering the discussion of intermolecular interactions through an unbiased identification of all close contacts. The Hirshfeld surface emerged from an attempt to define the space occupied by a molecule in a crystal to partition the crystal electron density into molecular fragments [40a]. Harshfeld surface analysis was performed using the Crystal Explorer program [40b].

2.6. TGA study

Thermogravimetric analysis (TGA) was carried out using a Perkin Elmer Pyris Diamond TG/DTA thermal analyzer in a nitrogen

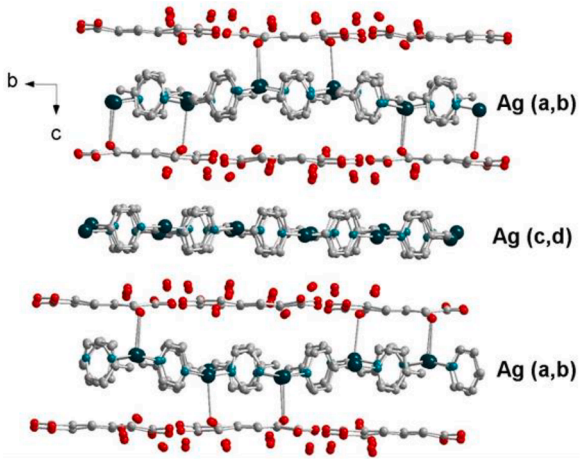

Fig. 1. Crystal packing viewed down axis a showing polymer that alternates with the plane of muconate anions and lattice water molecules.

atmosphere (flow rate: 50 cm^3 min^{-1}) at a temperature range 30–810 °C with a heating rate of 20 °C/min.

2.7. Study of photocatalytic property

The photocatalytic activity was evaluated towards methylene blue (MB) under UV light irradiation through a typical process. For this experiment, a standard solution (1 mM) of MB was prepared by dissolving 16 mg of solid MB in 50 mL water. Then 14.30 mg of complex **1** was added to 4 mL of the standard MB solution, and the mixture was stirred for 15 min to get the surface adsorption equilibrium of the compound in the dark. Then the solution was irradiated with UV 250 W high-pressure Hg lamp under stirring conditions up to the complete degradation of the dye. The photodecomposition of MB was studied with a UV-Vis spectrophotometer.

3. Results and discussion

3.1. Crystal structure description $\{[Ag_8(bpp)_8(H_2O)_3].(muc)_4.29(H_2O)\}_n$ (1)

The single crystal structural analysis of complex 1 (crystallizing in the monoclinic system, space group $P2_1/c$) evidences a supramolecular architecture (Fig. 1) consisting of cationic undulated 1D coordination polymers –[Ag(bpp)]$_n$- (bpp = 1,3-bis(4-pyridyl propane), extended in the direction of *b* axis. The chains are well separated and sandwiched by layers of water molecules and *trans, trans*-muconato (muc) anions linked by an extensive scheme of H-bonding.

Similar crystal networks have already been reported, for example, in $\{[Ag_3(bpp)_3(H_2O)_2](bpydc)_{1.5}.(H_2O)_6\}_n$ (H_2bpydc = 2,2'-bipyridine-5,5'-dicarboxylic acid)[36], $\{[Ag_2(bpp)_2(H_2O)](adip).(H_2O)_9\}_n$, (adip = adipate anions)[37], $\{[Ag_2(bpp)_2(H_2O)_2](CO_3)(H_3BO_3)_3.(H_2O)_2\}_n$[38], $\{[Ag_3(bpp)_3(ctc)].(H_2O)_{16}\}_n$, ($H_3$ctc = 1,3,5-cyclohexane-tri carboxylic acid) [41]. The formation of these architectures can be explained by Hard and Soft Acids and Bases (HSAB) theory [42], indicating silver atoms are preferentially coordinated by nitrogen ligands rather than carboxylate groups.

The asymmetric unit contains eight silver(I) ions, which form four cationic polymers with trivial differences in conformation, stacking in the *ab* plane. The arrangement is such that in one case, the sequence of polymers is –Ag(a)·Ag(b)-, while the other chains alternate in pairs, *i.e.*, -Ag(c)$_2$·Ag(d)$_2$- (Fig. 2). The Ag-N bond lengths fall in the range 2.107 (6)–2.149(6) Å (Table 1), with the metals spaced in the range 12.283–12.411 Å. However, out of eight silver atoms, Ag1a, Ag2a, and Ag2b are weakly coordinated at long distances by a water molecule (Ag-Ow of 2.660(6), 2.659(6), and 2.800(7) Å, respectively). This affects the geometry of the N-Ag-N angle for these metals that are in between 164.6 (3) and 167.2(3)°, while for other silver atoms, the N-Ag-N bond angles are almost linear (range 172.3(3)–179.0(3)°). The coordination geometries are in agreement with previous structures reported [16,41–43]. Of the different conformations (TT, TG, GG, and GG') that the bpp ligand can assume [45], here, the N-to-N distances of *ca.* 9.25 Å confirm an *anti–anti* (TT) conformation. No relevant π-π interactions are detected in the structure as the distance between ring centroids of the py rings is

Table 1
Selected coordination bond lengths (Å) and angles (°) for complex **1**.

Ag(1a)-N(4a)$^{\#1}$	2.137(6)	Ag(1c)-N(4c)$^{\#2}$	2.118(7)
Ag(1a)-N(1a)	2.149(6)	Ag(1c)-N(1c)	2.126(7)
Ag(2a)-N(3a)	2.137(6)	Ag(2c)-N(2c)	2.107(6)
Ag(2a)-N(2a)	2.140(6)	Ag(2c)-N(3c)	2.118(7)
Ag(1b)-N(1b)	2.108(6)	Ag(1d)-N(1d)	2.109(7)
Ag(1b)-N(4b)$^{\#2}$	2.124(7)	Ag(1d)-N(4d)$^{\#1}$	2.111(7)
Ag(2b)-N(3b)	2.117(6)	Ag(2d)-N(3d)	2.123(7)
Ag(2b)-N(2b)	2.119(6)	Ag(2d)-N(2d)	2.124(7)
Ag(1a)-O(1w)	2.660(6)	Ag(2b)-O(3w)	2.800(7)
Ag(2)a-O(2w)	2.659(6)		
N(4a)$^{\#1}$-Ag(1a)-N(1a)	164.6(3)	N(4c)$^{\#2}$-Ag(1c)-N(1c)	175.3(3)
N(3a)-Ag(2a)-N(2a)	166.0(3)	N(2c)-Ag(2c)-N(3c)	173.0(3)
N(1b)-Ag(1b)-N(4b)$^{\#2}$	172.3(3)	N(1d)-Ag(1d)-N(4d)$^{\#1}$	173.6(3)
N(3b)-Ag(2b)-N(2b)	167.2(3)	N(3d)-Ag(2d)-N(2d)	179.0(3)

Symmetry codes:.
$^{\#1}$) x-1, y, z.
$^{\#2}$) *x*+1, y, z.

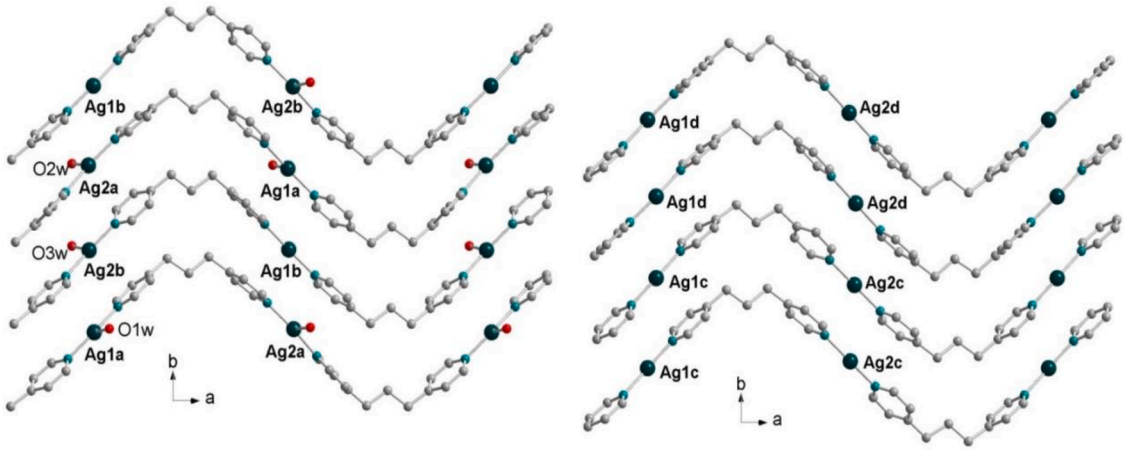

Fig. 2. Undulated polymers built by the eight independent silver ions.

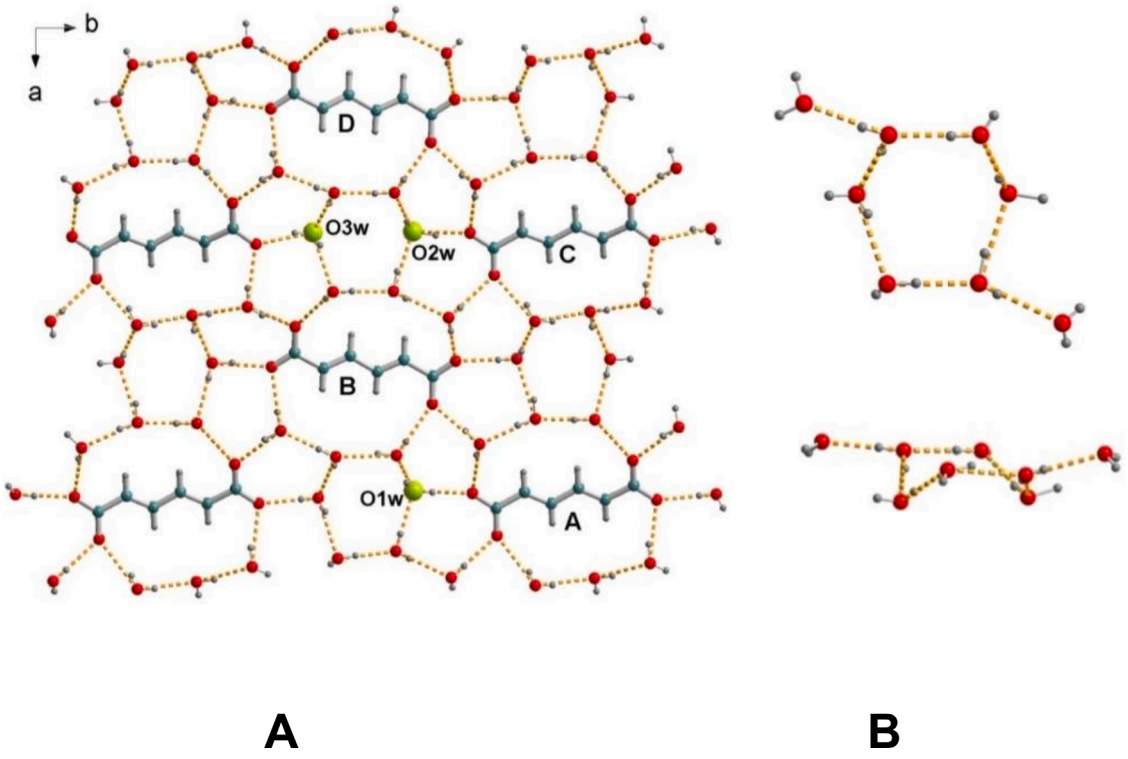

Fig 3. A. 2D hydrogen-bonded anionic layer in **1** formed by 29 water molecules and four muconate anions (A-D). The three green-colored water oxygens are those weakly coordinated to Ag atoms. B. Details of one of the octameric water clusters in the layer.

Table 2
Time-resolved decay parameters of BSA and BSA-complex **1** conjugate.

System	α_1	τ_1 (ns)	α_2	τ_2(ns)	α_3	τ_3(ns)	τ_{avg}(ns)	χ^2(best fitting)
BSA(10μM)	0.09	1.03	0.21	3.34	0.70	6.74	5.51	1.14
BSA+Complex**1**	0.11	0.802	0.27	4.03	0.61	6.85	5.35	1.10

larger than 4.23 Å. On the other hand, all pyridine moieties are involved in ring-Ag interactions with 3.30–3.62 Å distances.

Within the water–muc anionic layer, fully deprotonated dicarboxylate species act as counteranions to guarantee the electroneutrality of the whole structure. The 32 water molecules (29 lattices plus 3 coordinated to Ag ions) are orderly distributed and structured around the dicarboxylate anions (Fig. 3). Thus, the three aqua ligands participating in the H-bonding scheme reinforce the overall crystal structure. Despite a disagreement factor of *ca.* 8%, all H atoms of water molecules were detected in the difference Fourier map and gave rise to an ordered arrangement of H-bonding. The O···O distances vary from 2.696(8) to 2.907(11) Å (Table 2S), with an average value of 2.78 Å. It is worthy of note within the layer the formation of octameric water clusters, where the 6-membered ring of water oxygens assumes a distorted boat conformation (Fig. 3B), having the motif designated by a $R\,^{6}_{6}(12)$ graph-set notation [46]. It is evident that, as described earlier by Luo et al., the number of water molecules and the H-bonding pattern is governed by the different organic anionic templates [42–44].

3.2. Analysis of IR spectra

The IR spectrum of complex **1** revealed broadband (ESI) appearing in the 3200–3600 cm^{-1} due to ν(O-H) stretching [35b]. The $\nu(C^{3}_{sp}\text{-H})$ stretching vibration bands at 2920–2941 cm^{-1} are seen in the complex. Robust and sharp peaks at 1620 cm^{-1} and 1440 cm^{-1} may be due to carboxylate's asymmetric and symmetric vibration modes [35c]. Aromatic ν (Ar C=C) stretching band appears at 1370 cm^{-1}. A sharp band at 1042 cm^{-1} indicates the presence of ν(C-N) aliphatic stretching. It is further reported that the IR spectrum of the titled complex is recorded in the liquid state by dissolving the complex in 5% DMSO solvent. After comparing the results (ESI), it was evident that the complex has maintained its structure in the solution phase (in which its interaction with BSA was studied).

3.3. Hirshfeld surface analysis

The Hirshfeld surface and fingerprint plots have been used to evaluate the strength of close contacts and quantify weak intermolecular interactions in the 3D metal-coordination polymer. The present complex's asymmetric unit has been studied using this approach to illustrate the intermolecular interactions through a balanced identification of all close contacts. The representations are made transparent to support the observer in understanding the calculations by considering the view of the surrounding structural environment. The X-ray single crystal structure analysis demonstrated that the dicarboxylate muc anion is trapped between two Ag-bpp layers. The 3D Hirshfeld surface showed the presence of (A) O···H intermolecular H-bonding interactions, (B) H···H contacts, (C) C-H···C weak hydrophobic interactions, and, Ag···O(w) interactions (Fig. 4E) which are indicated in red colour on the Hirshfeld surface of Fig. 4. The corresponding level of the three significant interactions (a)–(c) is maintained in Fig. 4(D). From the structural analysis, it is observed that the muconate anion is stabilized with peripheral water molecules through extensive hydrogen bonding interactions. The Hirshfeld surface analysis justifies that the whole hydrogen-bonded network between the two layers is held by Ag···O(w) interactions

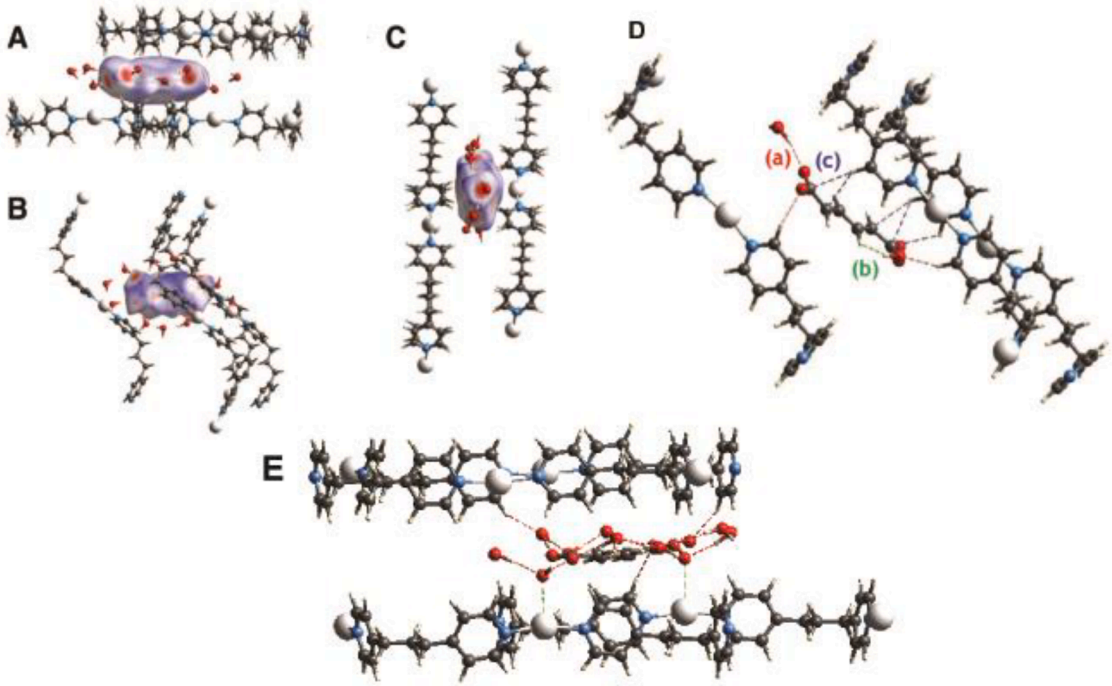

Fig. 4. The three-dimensional Hirshfeld surface of the free muc^{2-} species within the Ag polymers of the complex, plotted over d_{norm} *viewed* down (A) *a*-axis, (B) *b*-axis, (C) *c*-axis, and (D) Local (a) O-H·····O, (b) H·····H, (c) C-H·····C (hydrophobic) interactions of one free muc^{2-} anion in the complex, (E) Ag—O(w) interaction.

(Fig. 4E). The Hirshfeld surface analysis leads to the conclusion that the dicarboxylate species hold to the metal complex through different interactions, of which the most important contributions were that operative between H and O atoms of the Ag compound.

The corresponding 2D fingerprint plot (Fig. 5) indicates that O··H/H··O interaction account for 51.2% of the total Hirshfeld surface with a lower spike ($di = 1.3$, $de = 0.7$ Å) and upper spike ($di = 1.15$, $de = 1.4$ Å). Similarly, H···H interactions contribute 31.8 % with high concentration spiking at $di - de = 1.02$ and C··H/H··C interactions include 17% of the Hirshfeld surface spiking at $di = 1.34$, $de = 1.72$ Å, respectively. From the fingerprint plot, it is clear that O···H interaction contributes the most among all interactions.

3.4. Thermogravimetric analysis

To know the thermal stability of the titled complex thermogravimetric analysis (TGA) was performed on the powdered sample in a nitrogen environment in the temperature range of 30 °C to 810 °C. The TGA curve (Fig. S4) shows the dehydration process at 89°C, corresponding to the loss of thirty-two water molecules (weight loss 13.5%, calculating 16%), indicating the presence of coordinated and non-coordinated water molecules. The eventual step between 265°C and 395°C is associated with losing the bpp ligand with a weight loss of 45% (Calc. 44.2%). Then the 14.4% weight loss occurs for muc, (Calc. 15.9%) between 500°C and 590°C. Finally, the formation of residual Ag_2O (residue; experimental, 6.2%; calculating, 6.45%) [46]. The frameworks are stable up to 210 °C, providing decent stability [46].

3.5. Interaction with BSA

3.5.1. Steady-state fluorescence measurements

Fluorescence emission spectroscopy is one of the most powerful tools for studying the interaction of the synthesized polymeric complex with BSA *via* the quenching mechanism [47,48]. BSA has three domains, each containing two subdomains, with three types of fluorophores, *i.e.,* tyrosine (Tyr), tryptophan (Trp), and phenylalanine (Phe). The concentration of BSA was determined spectrophotometrically using a molar absorption coefficient of 43,824 M^{-1} cm^{-1} at 280 nm in 10 mM citrate-phosphate buffer at pH 7.4 [48]. The stock solution of Complex **1** was prepared by dissolving it in 10% DMSO solution. All fluorescence spectra were recorded in the citrate-phosphate buffer. Fluorescence studies were performed at a 12 μM concentration of BSA, while the concentration of complex **1** was varied from 0 to 11.43 μM. When BSA was excited at 295 nm, there was an emission maximum of around 340 nm, primarily due to the most crucial Trp-212 residue of the second domain [49–55] of BSA. Upon successive additions of complex **1,** a significant intrinsic fluorescence quenching of BSA was observed (Fig. 6A).

A systematic decrease of fluorescence intensity was observed with increasing concentrations of complex **1** without any significant alteration in the position of emission maxima. Since different quenching mechanisms, such as static or dynamic quenching or inner filter effect, can be responsible for the quenching of the fluorescence spectra [51], an inner filter correction was performed using the following equation:

$$F_{corr} = F_{obs} \times e^{\frac{(A_{exi}+A_{emi})}{2}}$$

F_{corr} and F_{obs} are the corrected and observed emission fluorescence intensities, respectively, and A_{emi} and A_{exi} are the absorbance values of the interacting species at emission and excitation wavelengths.

To assess the quenching mechanism, we used the Stern–Volmer equation:

$$\frac{F_0}{F} = 1 + K_q\tau_0[Q] = 1 + K_{SV}[Q] \quad (1)$$

where, F_0 and F are the fluorescence intensities of BSA in the presence and absence of complex **1**. K_q and K_{SV} are the bimolecular quenching rate constant and Stern–Volmer constant quenching constant, respectively. τ_0 is the average lifetime of the sample in the absence of a quencher, and [*Q*] is the concentration of the quencher, *i.e.,* complex **1**. The quenching constant K_q was evaluated to be $(3.18\pm0.0048) \times 10^{11}$, considering an average lifetime of 10^{-8} s (Fig. 6B). Literature data inspection reveals that the maximum limit of scattered collision quenching constant of various quenchers with the biopolymer is 2.0×10^{10}

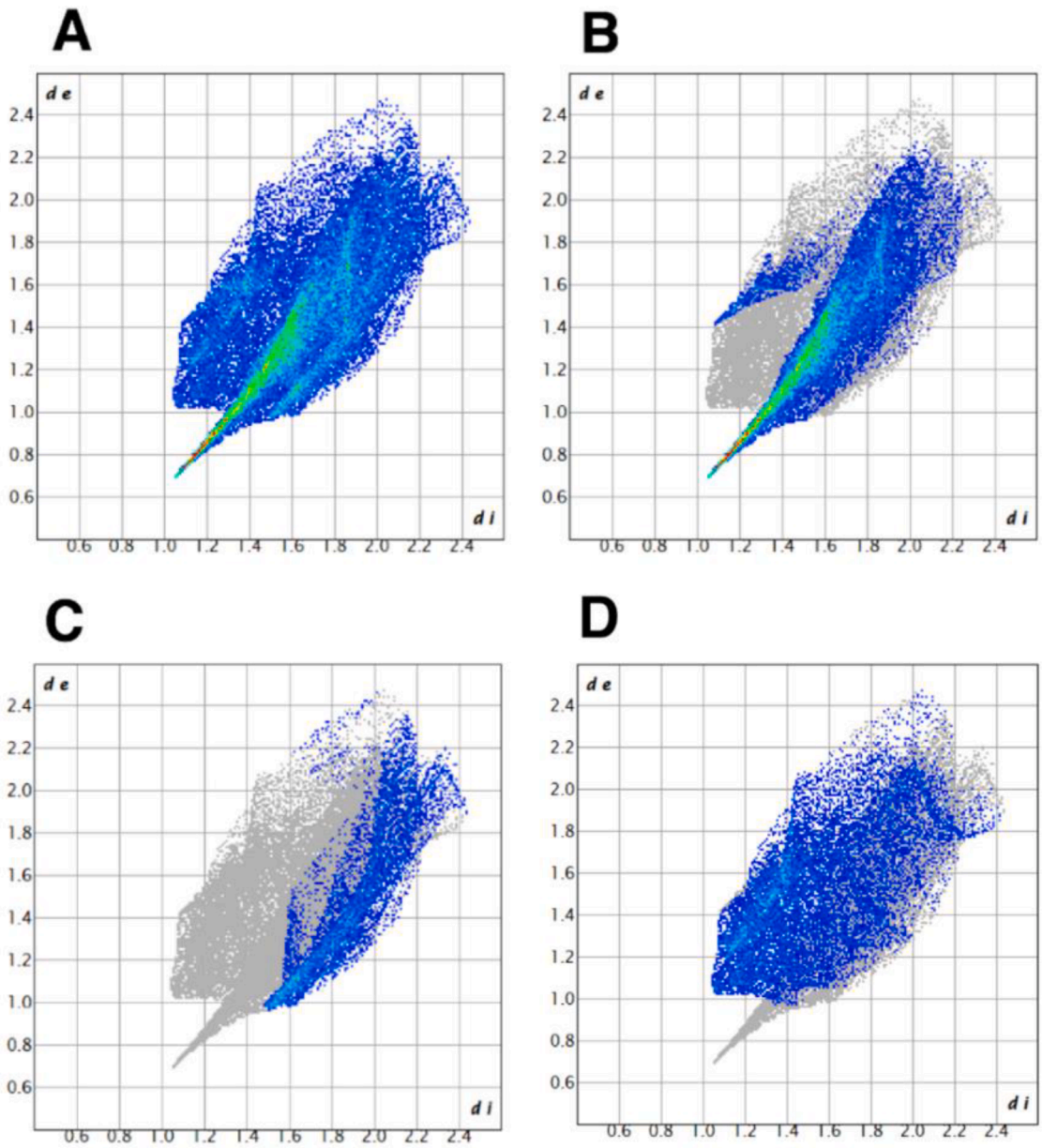

Fig. 5. 2D fingerprint plots: (A) Total, (B) O···H/H···O, (C) C···H / H···C (D) H···H interactions in the total Hirshfeld surface area.

[34–52]. The higher calculated value of K_q compared to the literature values indicated that the binding mechanism is static,*i.e.*, a ground state complex formation takes place between BSA and the complex [54,55]. Lifetime studies further justify it.

3.5.2. *Fluorescence lifetime study*

BSA has two fluorescence active tryptophan residues at positions 134 and 212[46]. So fluorescence lifetime measurement using Trp as the intrinsic probe is reliable for determining the quenching mode (static or dynamic) of BSA–complex **1** adduct [56]. The lifetime of BSA was measured before and after the addition of complex **1** (Fig. 6C). Time-resolved decay profile F(t) was determined through Horiba EZ time software using the following expression [57].

$$F(t) = \sum_{i=1}^{n} \alpha_i \exp\left(-\frac{t}{\tau_i}\right)$$

Here α_i and τ_i are the *i*th component's pre-exponential factors and excited state lifetime. For multi-exponential analysis, τ_{avg} is given by

$$\tau avg = \sum_{k=0}^{n} \alpha_i \tau_i$$

The experimental data of the fluorescence lifetime of BSA and BSA-Complex **1** were recorded using the Time-Correlated Single Photon Counting technique in a citrate-phosphate buffer. The fluorescence decay profile best fits the sum of three exponential functions with an average lifetime of 5.51 ns for pure BSA and 5.35 ns for the BSA-complex **1** conjugate [58,59]. The fluorescence lifetime of BSA in the absence and presence of complex **1** proved that ground-state complexation occurred between BSA and complex **1,** and the quenching was static. Time-resolved decay parameters of BSA and BSA-complex **1** conjugate are given in Table 2.

3.5.3. *Estimation of the binding constant and binding site*

After the establishment of the binding mechanism, the equilibrium binding constant and the number of binding sites were calculated using the following equation:

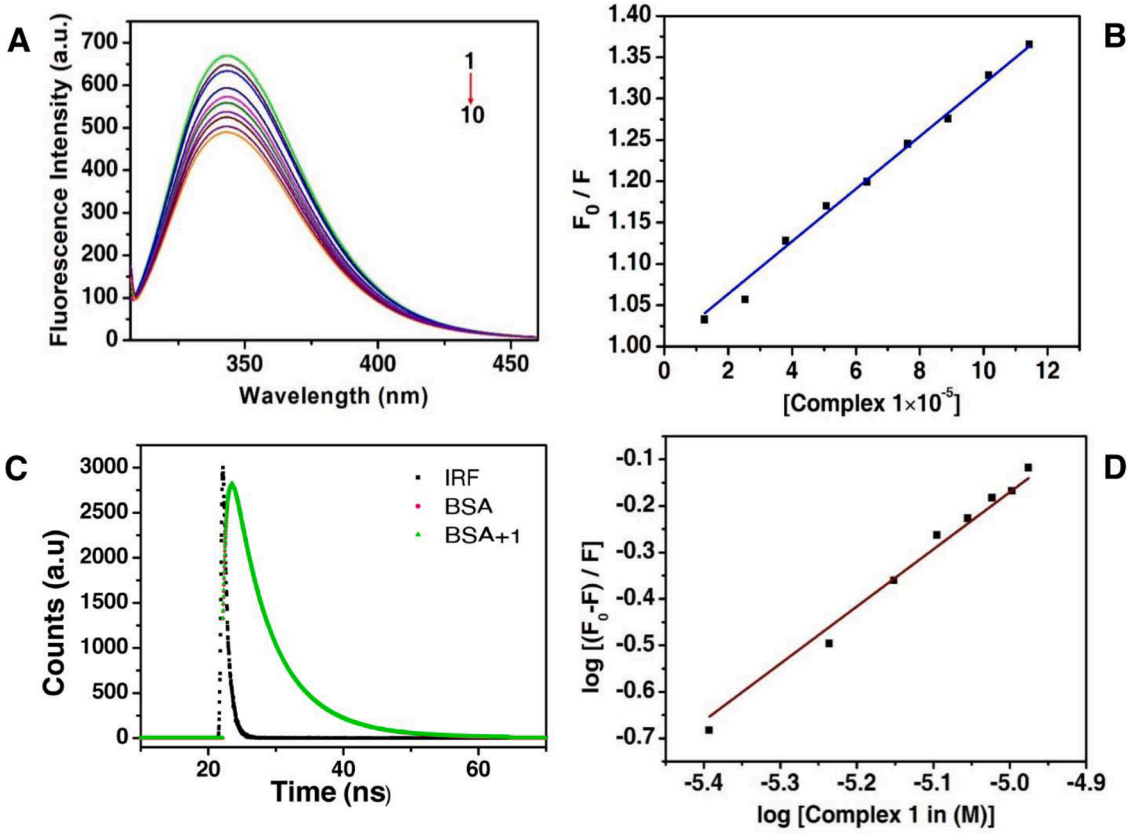

Fig. 6. (A) Fluorescence quenching spectra of BSA (12 μM, curve 1) on treatment with 1.1 μM complex **1** (2-10), (B) Stern–Volmer plot for binding of complex **1** with BSA, (C) Time-resolved decay profile of native BSA (10 μM) and BSA (10 μM) + **1** (1 μM) with instrumental resonance function (IRF), and (D) Estimation of binding constant of BSA and complex **1.**

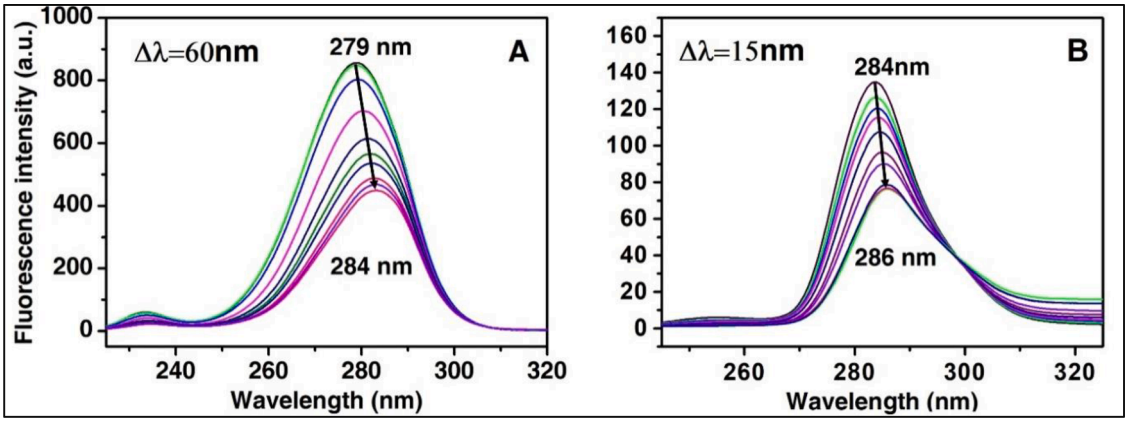

Fig. 7. Synchronous fluorescence spectra of BSA (A)Δλ=60 nm, (B) Δλ=15 nm.

$$log\frac{(F_0 - F)}{F} = logK_A + nlog[Q] \quad (2)$$

where, K_A and n are the binding constant and number of binding sites, respectively [60,61].

From the plot reported in Fig. 6(D), K_A and n were evaluated as (9.54 ±0.18) × 10^5 and (1.23±0.002), respectively, indicating cooperative binding between BSA and complex **1**.

3.5.4. *Synchronous fluorescence study*

Microenvironmental change in the vicinity of fluorophores can be studied with the help of synchronous fluorescence spectroscopy. The Δλ, *i.e.,* the difference between the excitation and emission wavelengths, determines the nature, shape, and intensity of synchronous fluorescence spectra. Synchronous fluorescence spectra yield information about the microenvironment around the Tyr residues at Δλ =15 nm, while at Δλ = 60 nm we get information about Trp residues [62,63].

Synchronous fluorescence spectra of BSA (10 μM) were quenched by complex **1** (Fig. 7) and showed a 5 nm red shift when Δλ operates at 60 nm in the citrate-phosphate buffer. This indicates that Trp residues of BSA are shifted towards a more hydrophilic core, which implies that it is more exposed to solvent, whereas, at Δλ=15 nm, there was a slight red shift. Thus, Tyr residues are less affected than Trp ones during the complexation process.

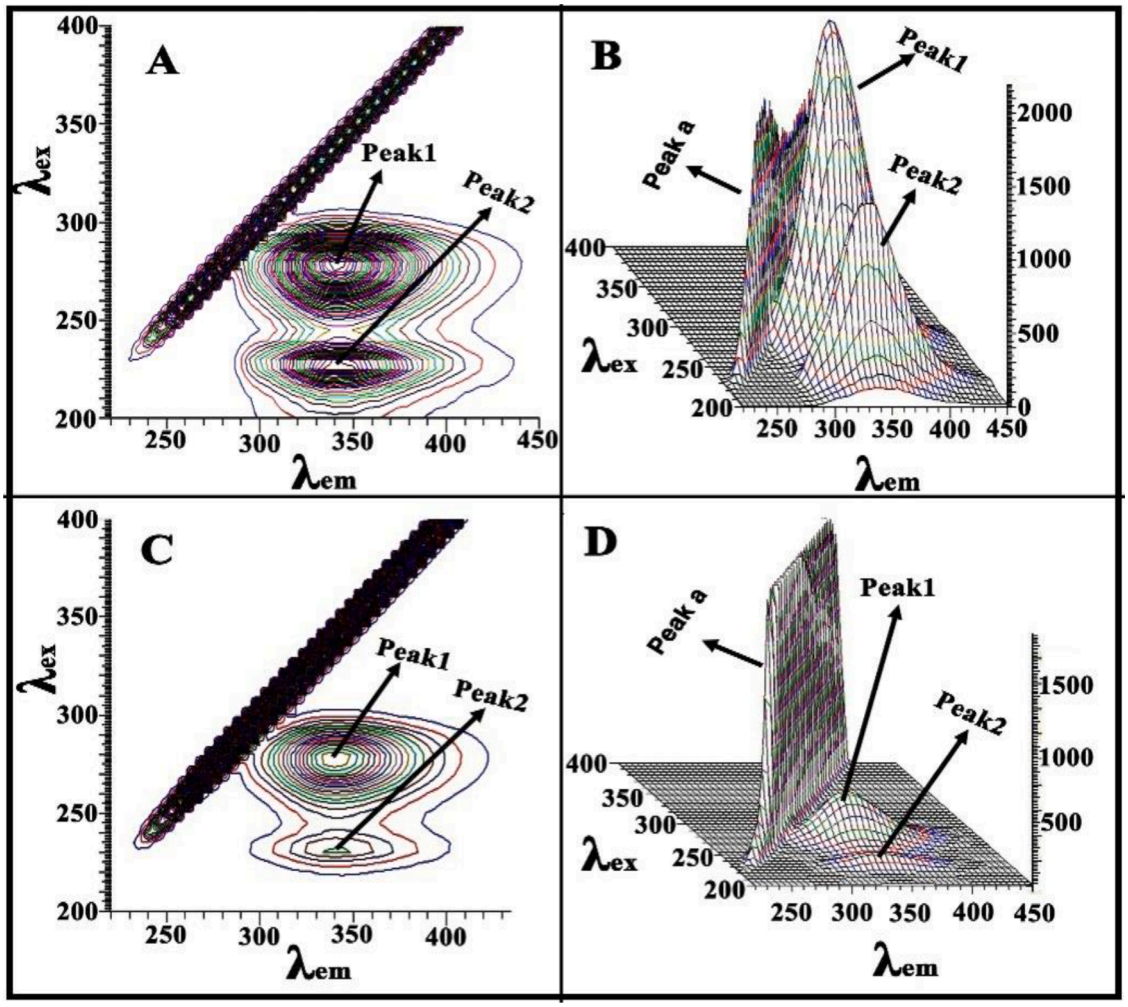

Fig. 8. 3D matrix contour (A and C) and bird's eye view (B and D) of BSA in the absence (above)and the presence of complex **1** (below).

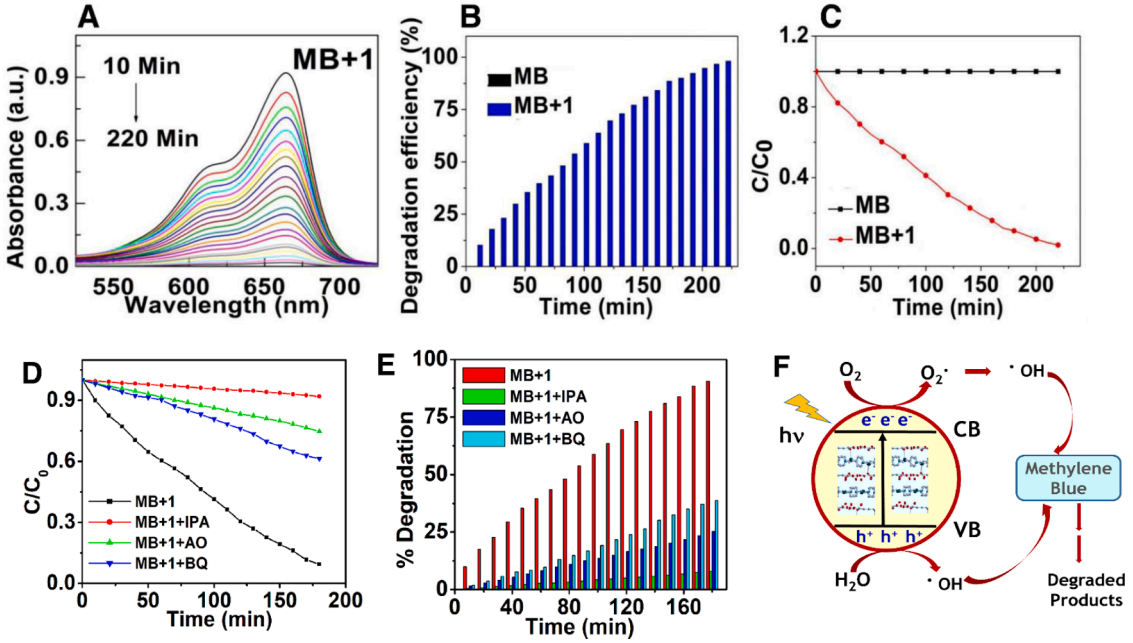

Fig. 9. (A) Absorption spectra of MB aqueous solution with complex **1** during irradiation, (B) Decrease in normalized absorption intensity of MB *vs.* time for **1**, (C) Comparison of the photodegradation efficiency *vs.* time under irradiation of complex **1**, (D) C/C_O plot of MB *vs.* time using IPA, AO, and BQ quenchers in the presence of complex **1**, (E). Trapping experiment of active species during photocatalytic degradation of MB dye, (F) Schematic representation of degradation of MB.

Table 3
Comparison of reported Ag(I) CPs based photocatalysts

Photocatalyst	Organic dye	Time (hours)	Degradation (%)	Refs.
Ag(I)-CP	MB	2	59	[70]
Ag(I)-CP	MB	3.5	56.9	[70]
Ag(I)-CP	MB	5	–	[70]
Ag(I)-CP	MB	6	54.8	[70]
Ag(I)-CP	MB	3.16	94	[70]
Ag(I)-CP	MB	3.6	98.06	This work

3.5.5. Spectroscopic analysis of excitation–emission matrix

3D fluorescence spectroscopy is an advanced method to study the conformational changes induced in the protein during BSA-ligand binding. The excitation-emission matrix was analyzed by comparing the emission intensity of an intrinsic fluorophore by simultaneously varying the excitation and emission wavelengths. Fig. 8A and B show the contour map and corresponding bird's eye mode of pure BSA (10 μM), respectively, and Fig. 8C and D represent that of the 1:1 BSA-complex **1** conjugate in the citrate-phosphate buffer. Peak "a" represents the Rayleigh scattering peak where $\lambda_{ex}=\lambda_{em}$ and appears due to the π-π* transition of the polypeptide backbone of BSA. Peak 1 (λ_{ex}= 278 nm; λ_{em}= 342 nm) is mainly due to Trp and Tyr residues of BSA, while peak 2 (λ_{ex}= 227 nm; λ_{em}= 343 nm) is generally due to n-π* transition of the amide group of the polypeptide backbone of BSA [58,64]. The 3D fluorescence spectra of BSA-complex **1** conjugate exhibited fluorescence quenching of peaks but no significant change in peak position. This study indicates the existence of sufficient binding interaction between complex **1** with Trp and Tyr residues of BSA without any apparent modification.

3.6. Study of photocatalytic behavior of the titled complex

3.6.1. Band gap energy calculation

Using Tauc's relationship, the optical band gap of a photocatalyst can be evaluated with the following equation [65]:

$$(\alpha h\nu)^n = C\left(h\nu - E_g\right)$$

where, α is the absorption coefficient of the semiconductor at a specific wavelength λ, h is Planck's constant, ν is the frequency of light, C is the proportionality constant, Eg is the energy difference between the valence band (VB) and conduction band (CB) and n = 1/2 and 2 for direct and indirect transition mode material, respectively. The band gap energy of complex **1** is calculated by extrapolating the plot of $(\alpha h\nu)^2$ vs. $h\nu$ (the photon energy) (Fig. S5). The band gap energy of complex **1** is 4.34 s eV.

3.6.2. Photocatalytic property

Methylene blue (MB) is one of the primary prevalent environmental organic dye pollutants in the textile industry due to its poor biodegradability and chemical stability [66,67]. Photocatalytic properties could be explored by photocatalytic degradation of organic dye under UV irradiation through a UV lamp (250 W). As the titled complex is insoluble in water, it was investigated as a heterogeneous catalyst for the degradation reaction of MB in water [68–70]. In the presence of complex **1**, the absorbance peak of MB declined continuously with time, as seen through the plot of (C/C_0) against time (Fig. 9). (C/C_0) values remain constant with time in the absence of a catalyst, while they decline when the catalyst is present. With complex **1,** the degradation efficiency of MB is 98.06% in 220 min, representing an excellent result against MB dye. Photocatalytic degradation of silver polymer follows first-order kinetics. So, using the relationship $\ln(C/C_0) = -kt$, where C_0 and C are the initial dye concentration and at instant t, respectively, and k is the rate constant. The degradation rate constant of **1** was calculated at 0.0179 min^{-1} [70], indicating a high catalytic activity for complex **1**. A comparison of some of the Ag(I) coordination polymer-based photocatalysts reported earlier, along with the titled complex is given in Table 3.

The purity and stability of the bulk material are essential for practical application. To confirm the virtue of the bulk for further catalytic studies, powder diffraction patterns were performed before and after the catalytic degradation study, which showed no significant change in the crystallinity of the complex (Fig. S6).

To find out the active species generated during the photocatalytic degradation of MB, the reactions were carried out in the presence of isopropyl alcohol (IPA), ammonium oxalate (AO), benzoquinone (BQ) that act as a scavenger for ȮH, H^+, $\dot{O}_2^-$, species, respectively [71–73]. The degradation efficiency of MB by complex **1** was strongly inhibited in the presence of IPA,[62,] whereas the effect of AO and BQ is lower. Therefore, we may conclude that ȮH is the species responsible for the photocatalytic degradation of dye (Fig. 9D and E).

During UV light irradiation, electron transfer from the valence band (VB) to the conduction band CB occurs in the complex, forming a hole (h+) in the VB. To offset their inequity, one electron from CB is trapped by O_2 to form $\dot{O}_2$ that is reduced further to form ȮH. The generated holes in VB induce the capture of one electron from H_2O to create active species ȮH that might degrade MB in the aqueous solution upon light irradiation (Fig. 9F).

4. Conclusion

A new Ag(I) coordination polymer comprising 1,3-bis(4-pyridyl propane (bpp) heterocyclic ligand and *trans, trans*-muconic acid anions is synthesized by sonication method and is successfully characterized by single crystal XRD study. The 3D Ag(l)-CP network is enforced by H-bonding, hydrophobic, and Ag-O interaction. Interestingly the Ag(l)-CPS showed a significant binding affinity towards protein BSA. Fluorescence emission spectra evidenced significant quenching with a K_q constant of $(3.18\pm0.0048) \times 10^{11}$, and fluorescence lifetime value indicated a static quenching. Quenching of BSA is also confirmed by the excitation-emission matrix (3D). From synchronous fluorescence spectral study, we find that Trp residues BSA are more exposed to the solvent system in the BSA-compound **1** complex. In addition, the Ag polymeric structure exhibited moderate catalytic activity towards the photodecomposition of methylene blue under UV irradiation following first-order kinetics.

Note

CCDC deposition No. 2234012 contains the supplementary crystallographic data for this paper. The data can be obtained from the Cambridge Crystallographic Data centre (CCDC): www.ccdc.cam.ac.uk.

Supplementary Information Summary: Absorption spectra of MB, Time-resolved decay profile, Lifetime profile, and IR spectra of the complex before and after the catalytic process.

CRediT authorship contribution statement

Laxmikanta Nandi: Methodology, Investigation, Software, Formal analysis. **Shovan Barman:** Methodology, Investigation, Software, Formal analysis. **Arindam Das:** Methodology, Investigation, Software, Formal analysis. **Paula Brandão:** Methodology, Investigation, Software, Validation. **Ennio Zangrando:** Methodology, Software, Validation, Formal analysis. **Anirban Basu:** Conceptualization, Supervision, Writing – review & editing. **Sudipta Dalai:** Conceptualization, Supervision, Validation, Writing – original draft, Writing – review & editing.

Declaration of Competing Interest

The authors declare that they have no known competing financial interests or personal relationships to influence the work reported in this paper.

Data availability

Data will be made available on request.

Acknowledgments

The authors thank UGC and DST, New Delhi, India, for providing special assistance and infrastructural support to the Department of Chemistry, Vidyasagar University, *via* SAP and FIST programs. USIC, Vidyasagar University, is gratefully acknowledged for providing instrumental facilities. We thank Dr. Subhasish Roy, BITS, Goa Campus, for his help with data analysis. Shovan Barman is thankful to UGC for providing a fellowship. Paula Brandão gratefully acknowledges the financial support of this work by the project CICECO-Aveiro Institute of Materials, UIDB/50011/2020, UIDP/50011/2020 & LA/P/0006/2020, financed by national funds through the FCT/MCTES (PIDDAC).

Supplementary materials

Supplementary material associated with this article can be found, in the online version, at doi:10.1016/j.molstruc.2023.136291.

References

[1] S. Kitagawa, R. Kitaura, S. Noro, Functional Porous Coordination Polymers, Angew. Chem Int. Ed. Engl. (43) (2004) 2334–2375.
[2] S.H. Lu, Y. Li, S.X. Yang, R.D. Zhao, Z.X. Lu, X.L. Liu, Y. Qin, L.Y. Zheng, Q.E. Cao, Three Silver Coordination Polymers with Diverse Architectures Constructed from Pyridine Carboxylic Hydrazide Ligands, Inorg. Chem. (58) (2019) 11793–11800.
[3] M.I. Rogovoy, A.S. Berezina, Y.N. Kozlova, D.G. Samsonenko, A.V. Artem'ev, Photoluminescence of Ag(i) complexes with a square-planar coordination geometry: the first observation, Inorg. Chem. Commun. (108) (2019) 7513.
[4] M.S. Chen, Z. Su, M. Chen, S.S. Chen, Y.Z. Lia, W.Y. Sun, Three-dimensional lanthanide–silver heterometallic coordination polymers: syntheses, structures and properties, CrystEngComm (12) (2010) 3267–3276.
[5] X. Lin, N.R. Champness, M. Schroder, Hydrogen, methane and carbon dioxide adsorption in metal-organic framework materials, Top. Curr. Chem. (293) (2010) 35–76.
[6] Y. Zhao, L. Luo, C. Liu, M. Chen, W.Y. Sun, Helical silver(I) coordination polymer with oxazoline-containing ligand: Structure, non-linear and ferroelectric property, Inorg. Chem. Comm. (38) (2011) 1145–1148.
[7] Y. Cui, Y. Yue, G. Qian, B. Chen, Luminescent functional metal–organic frameworks, Chem. Rev. (112) (2012) 1126–1162.
[8] A. Chira, B. Bucur, M.P. Bucura, G.L. Radu, Electrode-modified with nanoparticles composed of 4, 4′-bipyridine-silver coordination polymer for sensitive determination of Hg (II), Cu (II) and Pb (II), New J. Chem. (38) (2014) 5641–5646.
[9] X.F. Zheng, L.G. Zhu, Synthesis, structures and conductivity properties of silver 3-sulfobenzoate coordination polymers, Inorg. Chim. Acta. (365) (2011) 419–429.
[10] Z. Zhou, C. He, L. Yang, Y. Wang, T. Liu, C. Duan, Alkyne activation by a porous silver coordination polymer for heterogeneous catalysis of carbon dioxide cycloaddition, ACS Catal. (7) (2017) 2248–2256.
[11] X. Peng, X. Liu, J. Li, Li. Tan, RNA-binding of Ru(II) complexes $[Ru(phen)_2(7\text{-}OCH3\text{-}dppz)]^{2+}$ and $[Ru(phen)_2(7\text{-}NO_2\text{-}dppz)]^{2+}$: The former serves as a molecular "light switch" for poly(A)•poly(U), J. Inorg. Biochem. (237) (2022), 111991.
[12] F. Yuan, X. Liu, L. Tan, Binding and stabilization effect of arene ruthenium(II) polypyridyl complexes toward the triple-helical RNA poly(U)•poly(A)*poly(U), Inorg. Chim. Acta. (542) (2022), 121140.
[13] C.-L. Chen, B.-S. Kang, C.-Y. Su, Recent advances in supramolecular design and assembly of silver (I) coordination polymers, Aust. J. Chem. (59) (2006) 3–18.
[14] K. Uemura, Syntheses and crystal structures of novel silver (I) coordination polymers based on linear or tetrahedral coordination environments, Inorg. Chem. Commun. (11) (2008) 741–744.
[15] X. Li, L. Yang, C. Qin, F.-H. Liu, L. Zhao, K.-Z. Shao, Z.-M. Su, POM-based inorganic–organic hybrid compounds: synthesis, structures, highly-connected topologies and photodegradation of organic dyes, RSC Advances (5) (2015) 59093–59098.
[16] G.-G. Luo, D.-L. Wu, J.-H. Wu, J.-X. Xia, L. Liu, J.-C. Dai, Direct observation of conformational change of adipate dianions encapsulated in water clusters, CrystEngComm (14) (2012) 5377–5380.
[17] G. Lamming, J. Kolokotroni, T. Harrison, T.J. Penfold, W. Clegg, P.G. Waddell, Structural diversity and argentophilic interactions in one-dimensional silver-based coordination polymers, M.R. Probert, A. Houlton, Cryst. Growth Des. (17) (2017) 5753–5763.
[18] P. Halder, E. Zangrando, T.K. Paine, Self-assembly of silver (I) and bis-bidentate N, N-donor ligands: from a tetranuclear complex to coordination polymers, Dalton Trans. (27) (2009) 5386–5394.
[19] A.A. Thoppil, R. Sharma, N. Kishore, Complexation of β-lactam antibiotic drug carbenicillin to bovine serum albumin: Energetics and conformational studies, Biopolymer (89) (2008) 831–840.
[20] A. Chakrabarty, A. Mallick, B. Haldar, P. Das, N. Chattopadhyay, Binding interaction of a biological photosensitizer with serum albumins: a biophysical study, Biomacromolecules (8) (2007) 920–927.
[21] D. Tatlidil, M. Ucuncu, Y. Akdogan, Physiological concentrations of albumin favor drug binding, Phys. Chem. Chem. Phys. (17) (2015) 22678–22685.
[22] A. Basu, G.Suresh Kumar, Study on the interaction of the toxic food additive carmoisine with serum albumins: A microcalorimetric investigation, J. Hazard. Mater. (273) (2014) 200–206.
[23] A. Basu, G.Suresh Kumar, Thermodynamics of the interaction of the food additive tartrazine with serum albumins: A microcalorimetric investigation, Food Chem (175) (2014) 137–142.
[24] S. Ketrat, D. Japrung, P. Pongprayoon, Exploring how structural and dynamic properties of bovine and canine serum albumins differ from human serum albumin, J. Mol. Graphics Model (98) (2020), 107601.
[25] H. Xu, N. Yao, H. Xu, T. Wang, G. Li, Z. Li, Characterization of the Interaction between Eupatorin and Bovine Serum Albumin by Spectroscopic and Molecular Modeling Methods, Int. J. Mol. Sci. (14) (2013) 14185–14203.
[26] X. Hu, G. Li, J.C. Yu, Design, fabrication, and modification of nanostructured semiconductor materials for environmental and energy applications, Langmuir (26) (2010) 3031–3039.
[27] C.C. Chen, W.H. Ma, J.C. Zhao, Semiconductor-mediated photodegradation of pollutants under visible-light irradiation, Chem. Soc. Rev. (39) (2010) 4206–4219.
[28] H. Zhang, D. Chen, X. Lv, Y. Wang, H. Chang, J. Li, Energy-Efficient Photodegradation of Azo Dyes with TiO2 Nanoparticles Based on Photoisomerization and Alternate UV−Visible Light, Environ. Sci. Technol. (44) (2010) 1107–1111.
[29] A.D. Paola, E.G. Lopez, G. Marci, L. Palmisano, A survey of photocatalytic materials for environmental remediation, J. Hazard. Mater. (212) (2012) 3–29.
[30] H. Zhang, X.J. Lv, Y.M. Li, Y. Wang, J.H. Li, P25-graphene composite as a high performance photocatalyst, ACS Nano (4) (2009) 380–386.
[31] T.R. Gordon, M. Cargnello, T. Paik, F. Mangolini, R.T. Weber, P. Fornasiero, C. B. Murray, Nonaqueous synthesis of TiO_2 nanocrystals using TiF4 to engineer morphology, oxygen vacancy concentration, and photocatalytic activity, J. Am. Chem. Soc. (134) (2012) 6751–6761.
[32] M.J. Lopez-Munoz, J. Aguado, A. Arencibia, R. Pascual, Mercury removal from aqueous solutions of HgCl2 by heterogeneous photocatalysis with TiO_2, Appl. Catal. B: Environ. (104) (2011) 220–228.
[33] X.L. Wang, Q. Gao, A.X. Tian, G.C. Liu, Inserting $-(CH_2)_n-$ (n = 2, 3, 4) Spacers into the Reactant Mercapto-methyltetrazole Ligand for Tuning the Multinuclear AgI Clusters in Keggin-Based Compounds, Cryst. Growth Des. (12) (2012) 2346–2354.
[34] M.W. Chorab, V. Patroniak, M. Kubicki, G.K. Adziołka, J. Przepiorski, B. Michalkiewicz, Synthesis, structure, and photocatalytic properties of new dinuclear helical complex of silver (I) ions, J. Catal (291) (2012) 1–8.
[35] a) Y. Hu, F. Luo, F. Dong, Design synthesis and photocatalytic activity of a novel lilac-like silver-vanadate hybrid solid based on dicyclic rings of $[V_4O_{12}]^{4-}$ with $\{Ag_7\}^{7+}$ cluster, Chem. Commun (47) (2011) 761–763;
b) K. Nakamoto, Infrared Spectra of Inorganic and Coordination Compounds, John Wiley and Sons, New York, 1997;
c) X. Zhang, G.Y. Dong, Y.G. Liu, G.H. Cui, Syntheses, Structures and Catalytic Properties of Cobalt(II) and Silver(I) Coordination Polymers Based on Flexible Bis (2-methyl benzimidazole) and Dicarboxylic Acids, J Inorg. Organomet. Polym. Mater. (26) (2016) 62–68.
[36] Bruker (2007). Bruker AXS Inc., Madison, Wisconsin, USA.
[37] G.M. Sheldrick, A short history of SHELX, ActaCryst A (64) (2008) 112–122.
[38] L.J. Farrugia, J. Appl. Crystallogr. (32) (1999) 837–838.
[39] K. Brandenburg, Diamond Crystal (Ver 3.1), Crystal Impact GbR Bonn, Germany, 1999.
[40] a) M.A. Spackman, P.G. Byrom, A novel definition of a molecule in a crystal, Chem. Phys. Lett. (267) (1997) 215–220;
b) R.P. Spackman, M.J. Turner, J.J. McKinnon, S.K. Wolff, D.J. Grimwood, D. Jayatilaka, M.A. Spackman, CrystalExplorer: a program for Hirshfeld surface analysis, visualization and quantitative analysis of molecular crystals, J. Appl. Cryst. (54) (2021) 1006–1011.
[41] S. Kulovi, S. Dalbera, S. Dey, S. Maiti, H. Puschmann, E. Zangrando, S. Dalai, Polymorphism in [Ag(bpetan)]n Coordination Polymers with Nitrate and Isophthalate Anions: Photocatalytic and Antibacterial Activity, Hemolysis Assay and Study of Cytotoxicity, ChemistrySelect (3) (2018) 5233–5242.
[42] G.-G. Luo, D.-L. Wu, J.-H. Wu, L. Liu, J.-X. Xia, D.-X. Li, C. Peng, Z.-J. Xiao, J.-C. Dai, The first supramolecular water–borate–carbonate anionic rosette ribbon sandwiched by a Ag(I) cationic sinusoidal layer, Inorg. Chem. Comm. (15) (2012) 272–276.
[43] G.-G. Luo, S.-H. Wu, Z.-H. Pan, Z.-J. Xiao, J.-C. Dai, Inorg. Chem. Commun. (39) (2014) 34–38.
[44] R.G. Pearson, J. Songstad, Application of the Principle of Hard and Soft Acids and Bases to Organic Chemistry, J. Am. Chem. Soc. (89) (1967) 1827–1836.
[45] L. Carlucci, G. Ciani, D.M. Proserpio, S. Rizzato, CrystEngComm. (4) (2002) 121–129. L. Carlucci, G. Ciani, D.M. Proserpio, S. Rizzato,CrystEngComm. (4) 2002 121–129.
[46] a) M. Etter, Encoding and decoding hydrogen-bond patterns of organic compounds, Acc. Chem. Res. (23) (1990) 120–126;
b) A. Tabacaru, C. Pettinari, M. Busila, R.M. Dinica, New Antibacterial Silver (I) coordination polymers based on a flexible ditopic pyrazolyl-type ligand, Polymers (11) (2019) 1686–1703;

c) C.C. Chen, Y. Cai, L.F. Wang, Y.D. Wu, H.J. Yin, J.R. Zhou, C.L. Ni, W. Liu, Three Silver(I) Coordination Polymers Based on Pyridyl Ligands and Auxiliary Carboxylic Ligands: Luminescence and Efficient Sensing Properties, Inorg. Chem. (60) (2021) 5463–5473.
[47] Yan-Jun Wang, Rui-Ding Hu, Dong-Hua Jiang, Ping-Hua Zhang, Qiu-Yue Lin, Yun-Yun Wan, Synthesis, crystal structure, interaction with BSA and antibacterial activity of La (III) and Sm (III) complexes with enrofloxacin, J. Fluoresc. (21) (2011) 813–823.
[48] A.Y. Khan, M. Hossain, G.Suresh Kumar, Investigations on the interaction of the phototoxic alkaloid coralyne with serum albumins, Chemosphere (87) (2012) 775–781.
[49] B. Annaraj, C. Balakrishnan, M. Neelakantan, Synthesis, structure information, DNA/BSA binding affinity and in vitro cytotoxic studies of mixed ligand copper(II) complexes containing a phenylalanine derivative and diimine co-ligands, J. Photobiol. (160) (2016) 278–291.
[50] B. Li, J. Wang, H. Song, H. Wu, X. Chen, X. Ma, Synthesis, crystal structure, and BSA interaction with a new Co(II) complex based on 5-(trifluoromethyl)pyridine-2-carboxylic acid, J. Cord. Chem. (72) (2019) 2562–2573.
[51] J. Gu, G. Yang, X. Li, Q. He, X. Huang, T. Sun, Interaction mechanism of Cu^{+}/Cu^{2+} on bovine serum albumin: Vitro simulation experiments by spectroscopic methods, BioMetals (340) (2021) 493–510.
[52] N. Shahabadi, M. Maghsudi, Z. Ahmadipour, Study on the interaction of silver (I) complex with bovine serum albumin by spectroscopic techniques, Spectrochim. Acta, Part A: Mol. Biomol. Spectroscopy (92) (2012) 184–188.
[53] C.-Q. Jiang, M.-X. Gao, J.-X. He, Study of the interaction between terazosin and serum albumin: synchronous fluorescence determination of terazosin, Anal. Chim. Acta. (452) (2002) 185–189.
[54] Quenching of fluorescence by oxygen, Probe for structural fluctuations in macromolecules, J.R. Lakowicz, G. Weber, Biochemistry (12) (1973) 4161–4170.
[55] S. Tabassum, W.M. Al-Asbahy, M. Afzal, F. Arjmanda, R.H. Khanb, Interaction and photo-induced cleavage studies of a copper based chemotherapeutic drug with human serum albumin: spectroscopic and molecular docking study, Mol. BioSyst. (8) (2012) 2424–2433.
[56] E. Soliman, M.M. Ibrahim, M.E. El-Khoury, I. El-Mehasseb, A. El-Motaleb, M. Ramadan, M.E. Mahfouz, S.Y. Shaban, R. Eldik, BSA Interaction, Molecular Docking, and Antibacterial Activity of Zinc(II) Complexes Containing the Sterically Demanding Biomimetic N3S2 Ligand: The Effect of Structure Flexibility, Molecules (27) (2022) 3543.
[57] J.R. Lakowicz, Principles of Fluorescence Spectroscopy, 3rdedn, Springer, 2006, pp. 97–155.
[58] S. Das, A. Das, A. Maji, M. Beg, A. Singha, M. Hossain, A compact study on impact of multiplicative Streblus asper inspired biogenic silver nanoparticles as effective photocatalyst, good antibacterial agent and interplay upon interaction with human serum albumin, J. Mol. Liq. (259) (2018) 18–29.
[59] A.K. Bhunia, S. Saha, CuO Nanoparticle-Protein Bioconjugate: Characterization of CuO Nanoparticles for the Study of the Interaction and Dynamic of Energy Transfer with Bovine Serum Albumin, Bio NanoScience (10) (2020) 89–105.
[60] O.K. Abou-Zied, O.I.K. Al-Shihi, Characterization of subdomain IIA binding site of human serum albumin in its native, unfolded, and refolded states using small molecular probes, J. Am. Chem. Soc. (130) (2008) 10793–10801.
[61] F. Ding, J. Huang, J. Lin, Z. Li, F. Liu, Z. Jiang, Y. Sun, A study of the binding of CI Mordant Red 3 with bovine serum albumin using fluorescence spectroscopy, Dyes Pigments (82) (2009) 65–70.
[62] A. Naseri, S. Hosseini, F. Rasoulzadeh, M.-R. Rashidi, M. Zakery, T. Khayamian, Interaction of norfloxacin with bovine serum albumin studied by different spectrometric methods; displacement studies, molecular modeling and chemometrics approaches, J. Lumin. (157) (2015) 104–112.
[63] A. Basu, G.S. Kumar, Interaction and inhibitory influence of the azo dye carmoisine on lysozyme amyloid fibrillogenesis, Mol. Bio Syst. (13) (2017) 1552–1564.
[64] M. Sarkar, S.S. Paul, K.K. Mukherje, Interaction of bovine serum albumin with a psychotropic drug alprazolam: Physicochemical, photophysical and molecular docking studies, J. Lumin. (142) (2013) 220–230.
[65] C.W. Litton, D.C. Reynolds, Double-carrier injection and negative resistance in CdS, Phys. Rev.A (133) (1964) 536–541.
[66] S. Kulovi, L. Nandi, H. Puschmann, E. Zangrando, S. Dalai, Two 1D Silver(I) Coordination Polymers with 1,3-Bis(4-pyridyl) propane and Aromatic Carboxylate Anions: Synthesis, Structure and Photocatalytic Behavior, ChemistrySelect (6) (2021) 8950–8958.
[67] H.N. Chang, S.X. Hou, Z.C. Hao, G.H. Cui, Ultrasound irradiation effect on morphological properties of a 3D nano zinc (II) supramolecular coordination polymer, Ultason. Sonochem. (41) (2018) 67–74.
[68] P. Ristic, N. Filipovic, V. Blagogevic, J. Cirkovic, B.B. Hollo, V.R. Dokic, M. Donnard, M. Gulea, I. Marjanovic, O.R. Klisuric, T.R. Todorovic, 2D and 3D silver-based coordination polymers with thiomorpholine-4-carbonitrile and piperazine-1,4-dicarbonitrile: structure, intermolecular interactions, photocatalysis, and thermal behavior, CrystEngComm (23) (2021) 4799–4815.
[69] J.-C. Geng, L. Qin, X. Du, S.-L. Xiao, G.-H. Cui, Synthesis, Crystal Structures, and Catalytic Properties of Silver(I) and Cobalt(II) Coordination Polymers Based on Flexible Bis(benzimidazole) with Pyridine-2, 6-Dicarboxylate, Z. Anorg. Allg. Chem. (638) (2012) 1233–1238.
[70] K.V. Kumar, K. Porkodi, F. Rocha, Langmuir–Hinshelwood kinetics – A theoretical study, Catal. Commun. (9) (2008) 82–84.
[71] Y. MU, D. Wang, X.D. Meng, J. Pan, S. De Han, Z.Z. Xue, Construction of Iodoargentates with Diverse Architectures: Template Syntheses, Structures, and Photocatalytic Properties, Cryst. Growth Des (20) (2020) 1130–1138.
[72] A. Ajmal, I. Majheed, N. Malik, Principles and mechanisms of photocatalytic dye degradation on TiO2 based photocatalysts: a comparative overview, RSC Adv. (4) (2014) 37003–37026.
[73] N. Hussain, V.K. Bhardwaj, The influence of different coordination environments on one-dimensional Cu (II) coordination polymers for the photo-degradation of organic dyes, Dalton Trans. (45) (2016) 7697–7707.